



Dual role of magnetic ionic liquid in EMI absorbing polymer composites of P(VDF-TrFE) and *f*-MWCNTs

Anjana¹ · Amita Chandra¹

Received: 20 October 2022 / Accepted: 5 January 2023 / Published online: 21 January 2023
© The Polymer Society, Taipei 2023

Abstract

To enhance the EMI shielding capability in the X-band of a polymeric system (poly(vinylidene fluoride-trifluoroethylene)) P(VDF-TrFE) containing *f*-MWCNTs, magnetic ionic liquid (MIL) (1-butyl-3-methylimidazolium tetrachloroferrate ([Bmim][FeCl₄])) has been used in the present study. The porous structure formation due to the incorporation of the magnetic ionic liquid in the polymer has been seen in the scanning electron micrographs while the pore volume and their area has been measured using BET technique. The XRD, FTIR and RAMAN studies have thrown light on the interaction between the different constituents of the polymer composite. The synthesized polymer composite systems with 5 wt% of *f*-MWCNTs has high conductivity of $\sim 0.65 \text{ S.cm}^{-1}$ and moderate shielding effectiveness of $\sim 29.43 \text{ dB}$ at 8.2 GHz. The shielding effectiveness has been found to improve to $\sim 34 \text{ dB}$ on addition of 20 wt% of MIL of which the major contribution is due to the absorption mechanism (absorption loss $\sim 24 \text{ dB}$) which is attributed to the dielectric, magnetic and multiple reflection losses between interfaces. The above obtained result suggests that the MIL based polymer composite system having only *three* constituents, is a promising EMI absorbing material in the X-band due to the contribution of the MIL to both the conductivity and the magnetic loss.

Keywords Electromagnetic shielding effectiveness · Magnetic ionic liquid · Functionalized MWCNTs

Introduction

Technologically, the rapid development of communication and its extensive utilization in electronic devices (like local area network, military, radar systems, etc.) has created pollution/noise due to electromagnetic interference (EMI). The over exposure of this pollution is a potential threat for human health as well as for electronic devices [1–3]. This is likely to get more serious with the arrival of the 5G era. Hence, an intense effort is required to develop high-performance EMI shielding materials (such as plastics, ceramics, composites and functional materials). A good EMI shield material must have moderate conductivity, high dielectric constant and high magnetic loss. As all these properties cannot be envisaged in a single material, multi-component materials have been pursued. Traditionally, metal-based EMI shielding materials were preferred due to their high electrical conductivity [4, 5]. However, their application was limited

due to major drawbacks like corrosion, structural stiffness, high density and most importantly, ample surface reflection which sent back the EM waves in the surroundings/atmosphere. To overcome these problems, shield materials with polymer matrices having mostly carbon based fillers (e.g., multiwall carbon nanotubes, carbon fiber, graphene, and MXene, etc.) [6] were focused upon. Properties of these fillers like high mechanical stability, ultrahigh specific surface area, and high conductivity [7] were the reasons for their preferred usage. Also, magnetic nanoparticles have been used as fillers (e.g., Fe, Co, Ni, ferrite, and alloys) [8] as they provide large magnetic losses. In EMI shielding mechanism, both dielectric and magnetic fillers play significant roles in dissipating EM energy through dielectric and magnetic losses [9, 10]. Kim et al. [11] have reported shielding effectiveness (SE) with MWCNTs containing Fe catalyst in PMMA polymer matrix of $\sim 27 \text{ dB}$ while Che et al. [12] have reported SE of $\sim 25 \text{ dB}$ in Fe encapsulated with CNTs. Kallumottakkal et al. [13] have reported $\sim 43 \text{ dB}$ SE in CoFe in PU matrix.

As MWCNTs possess many exceptional properties like high mechanical strength and conductivity, light weight, low density and high aspect ratio, they are mostly used

✉ Amita Chandra
achandra@physics.du.ac.in

¹ Department of Physics and Astrophysics, University of Delhi, 110007 Delhi, India

in the field of EMI shielding [7]. However, the carbon nanofillers have a tendency to aggregate in polymeric matrix due to the strong intrinsic Van der Waals attractive force [14–16] making it difficult to disperse. Therefore, for proper dispersion as well as interfacial interaction between MWCNTs and the polymeric matrix, various techniques (e.g., ultrasonication, surface modification) have been used. For surface modification of MWCNTs, chemical functionalization (covalent and non-covalent bonding techniques) and oxidative acid treatments have been reported [17, 18]. This study has used the oxidative acid treatment for functionalization.

It is well known that the absorption of EM waves is based on the change of these waves into heat or another type of energy and/or radiation [19, 20]. This is achieved via the shield material's electric and/or magnetic dipoles ability to interact with the EM wave. Normally, the polymer matrices are insulating in nature through which the EM waves can pass through. Also, they have low density, can be made very thin and flexible. The ever decreasing size of modern day electronics and telecommunications devices requires flexible materials which can be moulded into desired shapes and sizes. Polymer matrices fulfil all these requirements. The work in this paper is on polymer composites using the polymer polyvinylidene fluoride-trifluoroethylene (P(VDF-TrFE)). P(VDF-TrFE) [21–23] has attracted much attention of scientist/technologists as it exhibits piezoelectric, pyroelectric and ferroelectric properties. Many studies are available on PVDF and its copolymers being exploited in modern electronic devices for energy storage and harvesting applications. The five crystalline phases (viz., α , β , γ , δ , and ϵ) of PVDF can be obtained by varying the synthesis process. Among these, the β -phase has ferroelectric properties. In the case of its copolymer, P(VDF-TrFE), the β -phase being inherently present gives it a ferroelectric nature [24–27]. The high dielectric constant of (P(VDF-TrFE) 70/30 mol%) makes it a good choice as EMI shielding material.

Another viable novel approach is using magnetic ionic liquids (MILs) in the polymer matrix having MWCNTs. MILs are room temperature ionic liquids (RTILs) and obtained by the incorporation of a paramagnetic component as either the cation or anion in the IL structure [28, 29]. MILs are attracting much attention over the conventional ILs due to their ability to exhibit permanent magnetic response to an external magnetic field without the need of further adding magnetic particles as the magnetic properties originate either from the anion or cation or from both [30–32]. The magnetic, electrical, mechanical and electromechanical properties of MILs have been enlisted in an earlier study [33]. These MILs can be used as alternative to magnetic fillers as they have the added advantage of enhancing the mobile charge carrier density (and thereby conductivity) of the material along with the magnetic losses. Kowsari et al.

[34] have reported MIL (1-methylimidazolium tetrachloroferrate) conducting GO/epoxy resin composites and found the SE to be ~ 25.21 dB in X-band.

The main focus of this work is to develop a class of MIL based polymer composites using the host matrix of P(VDF-TrFE) dispersed with f-MWCNTs. EMI shielding materials based on (Poly(vinylidene fluoride-trifluoroethylene) P(VDF-TrFE)/f-MWCNTs/1-butyl-3-methylimidazolium tetrachloroferrate ([Bmim][FeCl₄])) have been synthesized and characterized. With the addition of f-MWCNTs in the pristine P(VDF-TrFE), conductivity as high as 0.65 S.cm^{-1} has been achieved which is credited to the formation of the connecting pathways by the f-MWCNTs and large interfacial area between the host matrix and the f-MWCNTs. The incorporation of MIL in the above polymer composite imparts it the following properties; (i) provides additional free charge carriers for conduction, (ii) improves magnetic losses, and (iii) enhances the porosity (leading to multiple scattering of EM waves). Here, the addition of 20 wt% of MIL in the polymer composite has given a total shielding effectiveness (SE_T) of ~ 34 dB in X-band (corresponding to maximum absorption loss (~ 24 dB)). This enhancement in SE can be attributed to the magnetic losses, multiple reflection losses, and dielectric losses.

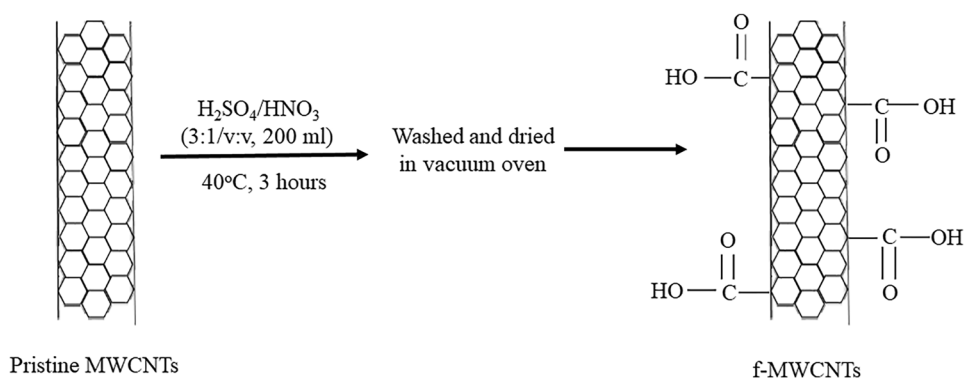
Experimental section

Preparation of functionalized MWCNTs

Acid treatment has been used for the surface modification of the pristine MWCNTs (50–90 nm diameter and $\geq 95\%$ carbon basis, procured from Sigma Aldrich, USA). Oxygen containing groups (viz., carboxyl groups) have been introduced onto the surfaces of pristine MWCNTs. Initially, the pristine MWCNTs (1.0 g) have been taken in a glass plate and added to a 200ml solution of nitro-sulfuric acid [(3:1 ratio (v:v) mixture of H₂SO₄ (98%)/HNO₃ (68%)]. Thereafter, the above solution has been ultrasonicated (at 40 °C) for 3 h. Then, the mixture has been filtered and washed with deionized water (4–5 times) till a pH of ~ 7 is attained. The obtained product has been dried in a vacuum oven at 70 °C for 24 h. Finally, functionalized MWCNTs (f-MWCNTs) have been obtained. The schematic representation of the above functionalization process has been shown in Fig. 1.

Synthesis of polymer composites

Polymer composites have been prepared using the solution cast technique. In this technique, first, the polymer (P(VDF-TrFE), 70:30 mol in powder form procured from Sigma Aldrich, USA) has been dissolved in acetone at 45 °C and then continuously stirred for 6 h using a magnetic stirrer. The

Fig. 1 Schematic of surface modification of pristine MWCNTs

f-MWCNTs dispersed in acetone are then ultrasonicated for 1 h before adding to the polymer solution. This mixture is again stirred for 6 h at 45 °C. The resulting solution is then poured into Petri dishes. The solvent evaporates at room temperature in a few days and a dry film is obtained. The optimized weight% of P(VDF-TrFE):f-MWCNTs has been found to be 1:5 corresponding to the highest EMI shielding property.

In this optimized P(VDF-TrFE):f-MWCNTs mixture, now different amounts (10, 20, and 30 wt%) of the magnetic ionic liquid (1-butyl-3-methylimidazolium tetrachloroferrate) [Bmim][FeCl₄] (purity ≥ 98.0%, $M_w \approx 336.88$ g mol⁻¹, purchased from TCI Chemicals (India) Pvt. Ltd) has been added. This mixture has been stirred for 4 h at 45 °C. Like above, the obtained solution has been poured into Petri dishes and left to dry for 3-4 days at room temperature.

Before characterization of the prepared films, they have been vacuum dried at 10⁻³ torr for 4-5 days to remove traces of moisture/solvent giving free-standing flexible films. The schematic of the entire procedure is shown in Fig. 2. Also, the codes for the prepared samples along with their respective composition are given in Table 1.

It is to be noted that due to the following two reasons, the MIL remains confined in the polymer matrix: (i) MILs are known to have very high viscosity which helps in containing them within the pores and (ii) when MIL enters the pores, electrostatic interactions occur between the MIL's ions and the polymeric matrix dispersed with f-MWCNT attributed to the presence of charges in its structure and ease of formation of hydrogen bond (due to the presence of OH⁻ groups and H terminations) and π - π interactions (i.e., cyclic structure and double bonds) [35].

Characterization

Powder XRD data has been obtained using Shimadzu D8 DISCOVER X-ray diffractometer. Raman-scattering measurements have been done (at room temperature) using a Renishaw micro-Raman system with a grating of 2400 lines/mm. Fourier transform infrared (FTIR) spectra have been

recorded in transmission mode using PerkinElmer FTIR infrared spectrometer in the range 4000-400 cm⁻¹ having resolution 2 cm⁻¹ to investigate the nature of the chemical bonds. Magnetic studies of the MIL and composite films have been investigated (at room temperature) using Vibrating Sample Magnetometer (VSM) (The Microsensors ADE-Model EV9) in an external field up to 1 kOe. The surface morphology of the P(VDF-TrFE)/f-MWCNTs/[Bmim][FeCl₄] films has been obtained with a Scanning Electron Microscope (SEM, JEOL, JSM 5600) operated at accelerating voltage between 10 and 30 kV. Thermal studies of the polymer composites have been done in N₂ atmosphere (at heating rate 10 °C/min) by using Thermo Gravimetric Analysis (TGA) equipment from Perkin Elmer. The ionic conductivity has been determined using Electrochemical Impedance Spectroscopy (EIS) measurements at room temperature. To investigate the electromagnetic shielding parameters, dielectric studies, and magnetic studies in the X-band (8.2–12.4 GHz) at room temperature, Agilent E8362B Vector Network Analyzer has been used. To obtain the EMI shielding parameters and dielectric properties, rectangular strips of polymer composites films have been placed inside the sample holder with dimensions 28 mm x 13 mm x 2.6 mm (length x width x thickness).

Results and discussion

Structural studies and surface morphology of MWCNTs and f-MWCNTs

Figure 3i shows the XRD profiles of pristine MWCNTs and f-MWCNTs. In Fig. 3i, the characteristic peaks for pristine MWCNTs have been observed at 25.99° [002], 43.03° [100] and 54.40° [004] while these peaks appear at 25.44° [002], 43.30° [100] and 54.22° [004], respectively, for f-MWCNTs [36, 37]. The diffraction peaks at 25.9° and at 25.4° both correspond to pristine MWCNTs and f-MWCNTs exhibiting the hexagonal graphite structure [38]. This observation shows that although the acid treatment of pristine MWCNTs does

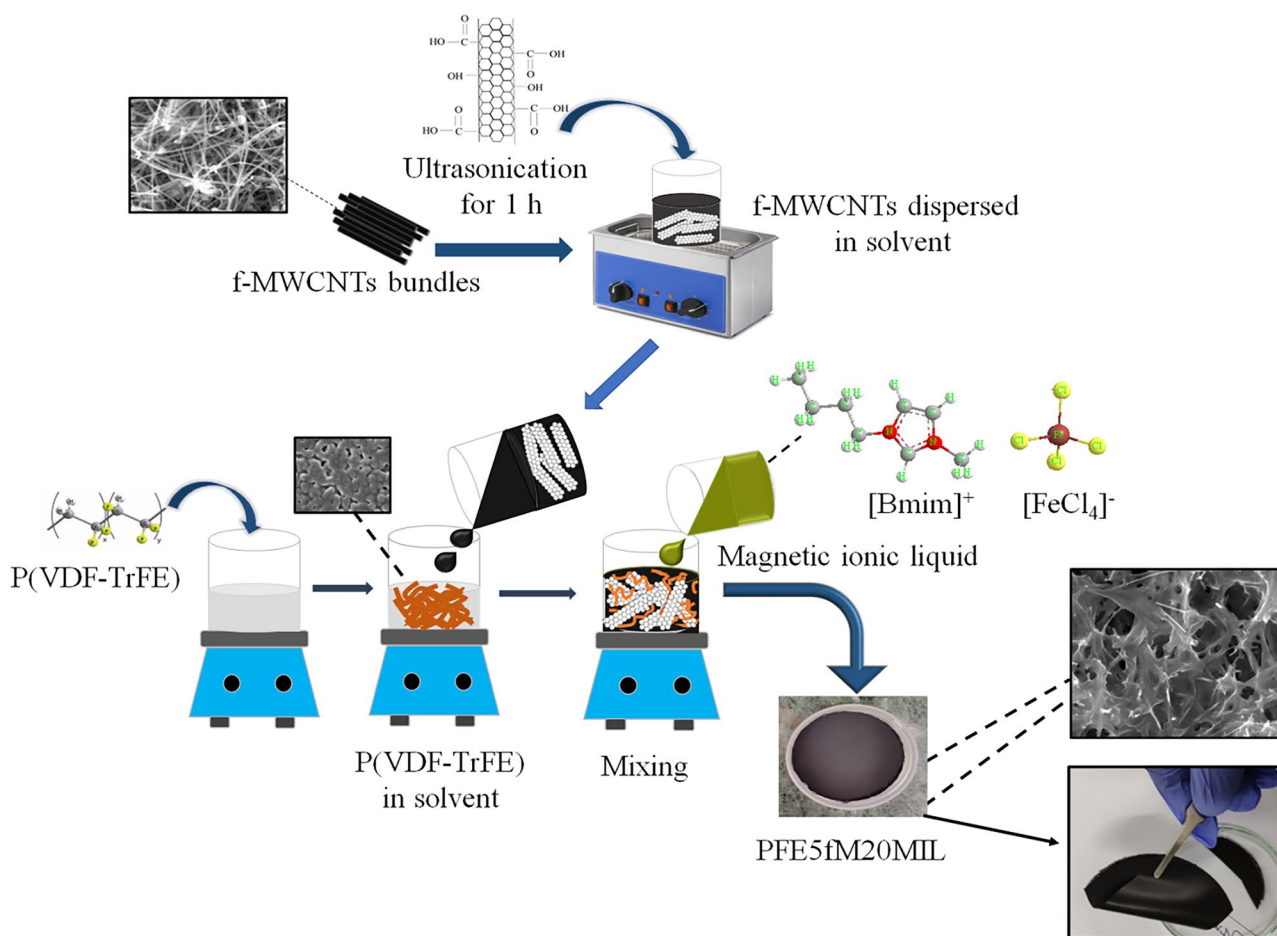


Fig. 2 Fabrication steps for obtaining composite films

not change its nanotube like structure [38], it does enhance the peak intensity in f-MWCNTs. This increase in intensity shows a highly graphitized (crystalline) structure of the f-MWCNTs as reported earlier [39].

Figure 3iia-b show the surface morphology of acid-treated MWCNTs along with pristine MWCNTs. It can be seen that acid treatment has resulted in the f-MWCNTs having nanotubes which are randomly and loosely entangled while the pristine MWCNTs have a higher level of aggregation. Additionally, the morphology of functionalized MWCNTs is found to remain intact even after acid treatment.

To know the possible conformational changes and to confirm the attachment of functional groups at the surface of MWCNTs, FTIR has been used. The FTIR spectra of (a) MWCNTs and (b) f-MWCNTs have shown in Fig. 3iii. The band at 1745 cm^{-1} corresponds to the C=O stretching vibration of $-\text{COOH}$, curve (b), which confirms that the $-\text{COOH}$ groups were attached with MWCNTs. The peak at 3423 cm^{-1} is ascribed to the $-\text{OH}$ stretching of $-\text{COOH}$ groups, present on the nanotube surface [40]. The presence of the above functional groups at the surface of f-MWCNTs confirms the surface modification of MWCNTs.

Table 1 Compositions of the P(VDF-TrFE)/f-MWCNTs/MIL composites system

Sample Name	Polymer composites	Weight ratio
P(VDF-TrFE)	P(VDF-TrFE)	100
PFE5fM	P(VDF-TrFE):f-MWCNTs [1:0.05]	95 + 5
PFE5fM10MIL	P(VDF-TrFE):f-MWCNTs:[Bmim][FeCl ₄] [(1:0.05) + 10 wt%]	85.7 + 4.3 + 10
PFE5fM20MIL	P(VDF-TrFE):f-MWCNTs:[Bmim][FeCl ₄] [(1:0.05) + 20 wt%]	76.2 + 3.8 + 20
PFE5fM30MIL	P(VDF-TrFE):f-MWCNTs:[Bmim][FeCl ₄] [(1:0.05) + 30 wt%]	66.7 + 3.3 + 30

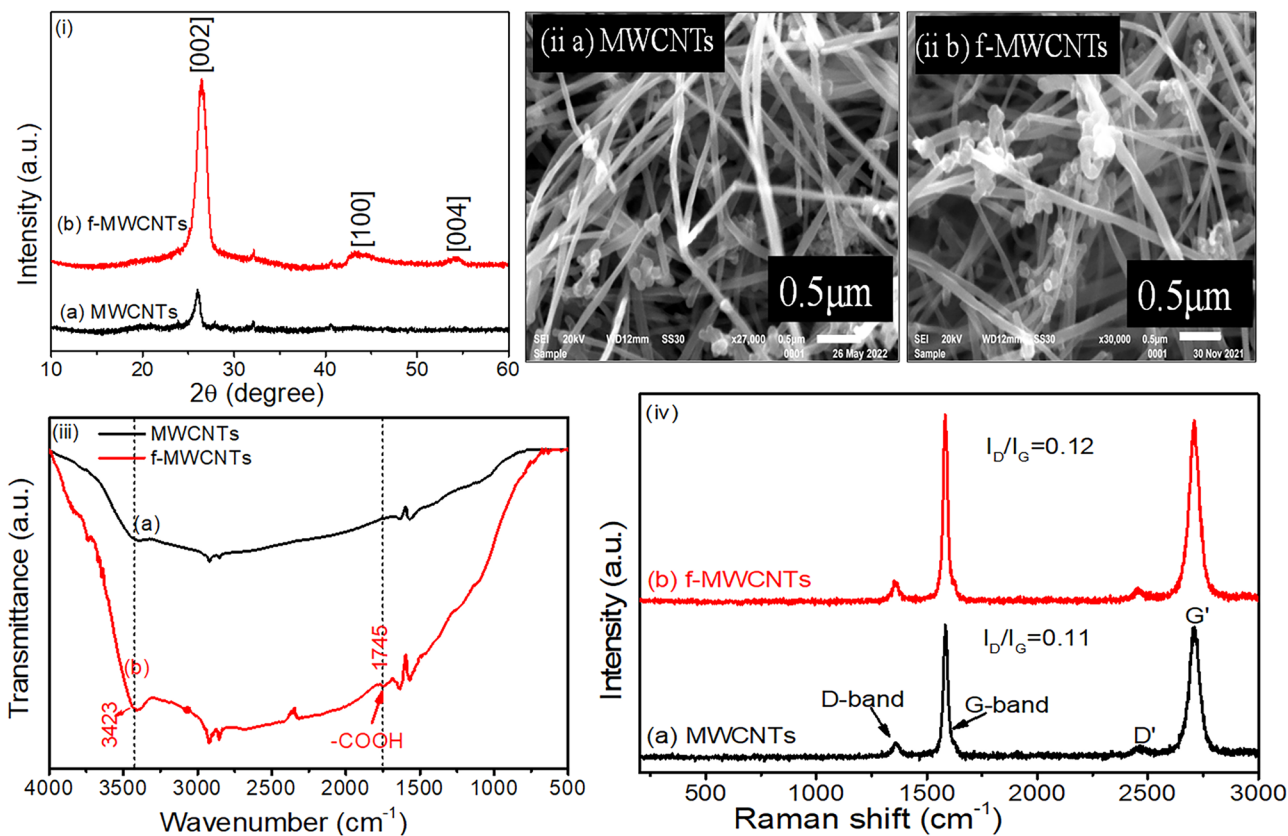


Fig. 3 i XRD, ii SEM images, iii FTIR study, and iv Raman spectra of pristine MWCNTs and f-MWCNTs

The Raman spectra of the pristine MWCNTs and f-MWCNTs are shown in Fig. 3iv. The characteristic peaks located at $\sim 1356\text{ cm}^{-1}$ (D-band), $\sim 1582\text{ cm}^{-1}$ (G-band), $\sim 2454\text{ cm}^{-1}$ (D'-band) and $\sim 2707\text{ cm}^{-1}$ (G'-band) of pristine MWCNTs are seen in Fig. 3iva. The D band indicates the amorphous

nature of carbon which may be due to the structural defects/vacancy present in the graphitic structure. The stretching in the graphitic plane which leads to tangential shear mode of carbon atoms is reflected in the G-band [41–43] whose strength is either due to the amount of disordered graphite or

Table 2 Assignment of the vibrational modes of P(VDF-TrFE), [Bmim][FeCl₄] and polymer composites

Wavenumber (cm ⁻¹)	P(VDF-TrFE)	[Bmim][FeCl ₄]	PFE5fM	PFE5fM10MIL	PFE5fM20MIL	PFE5fM30MIL
Aromatic C–H vibrations of [Bmim] ⁺ cations		619, 647, 1162, 3148	-	-	-	-
Aliphatic C–H vibrations of [Bmim] ⁺ cations		831, 740, 1462, 2961, 2934	-	738, 1452	738, 1458	738, 1461
CF ₂ symmetric stretching	840	-	840	840	840	840
CF ₂ anti-symmetric stretching, CH ₂ rocking	880	-	879	878	879	879
CH ₂ wagging, C–C stretching	1076	-	1075	1075	1076	1075
CH ₂ rocking, CF ₂ anti symmetric stretching	1165	-	1167	1168	1163	1162
CH ₂ scissoring, C–C stretching, CF ₂ symmetric stretching	1283	-	1282	1282	1282	1282
CH ₂ wagging, C–C stretching	1402	-	1398	1398	1398	1398
C–C and C–N bending vibrations in [Bmim][FeCl ₄]	-	1563	-	1565	1566	1563

the conjugation disruption in the graphene sheet [44]. After the functionalization of MWCNTs, the position of the bands (D, G, D', and G') is shifted towards higher wave numbers ($\sim 2\text{-}3\text{ cm}^{-1}$) as shown in Fig. 3ivb. This shift may be due to the breaking of bonds and/or attached chemical groups which can lead to defects in the structure. These observed shifts in bands once again, confirm that the oxidation groups do not damage the graphitic structure of MWCNTs [45, 46] on functionalization. Also, for quantification of disorder in the structure, the intensity ratio of the D and G bands (I_D/I_G , i.e., R) has been calculated and given later in Table 2. This value of R is less for MWCNTs in comparison to the f-MWCNTs. The obtained value of R confirms that covalent functionalization results in higher structural defects in the f-MWCNTs.

Structural studies and surface morphology of composite films

XRD studies

Figure 4 shows the XRD patterns of different composite films. In Fig. 4a, the prominent peaks of polymer P(VDF-TrFE) appear at 19.5° [110/220], 34.48° [001], and 40.53° [201] overriding a broad halo in the range $10^\circ\text{-}45^\circ$ which are associated with the β -phase of the polymer [47]. The addition of f-MWCNTs in the P(VDF-TrFE) matrix shows a slight reduction in the intensity of all the peaks along with the appearance of a new peak at $2\theta \sim 27.2^\circ$ [002], a signature of f-MWCNTs. The minor shift in diffraction peaks may be due to the complex formation between the P(VDF-TrFE) and f-MWCNTs, Fig. 4b-e. Further, with the incorporation of MIL in the PFE5fM film, an additional new peak is seen at $2\theta \sim 29.45^\circ$ (JCPDS file No. 00-001-1059) (which is of FeCl_3) and marked by '*' in Fig. 4c. However, on further

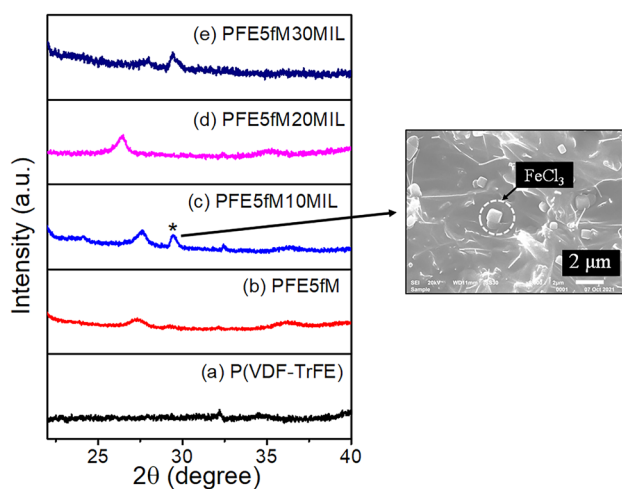


Fig. 4 XRD patterns of **a** P(VDF-TrFE), **b** PFE5fM, **c** PFE5fM-10MIL, **d** PFE5fM20MIL, and **e** PFE5fM30MIL composite films

(> 10 wt%) addition of MIL, this peak is found to disappear. This observation can be corroborated with the SEM studies given below. On increasing the MIL content to 30 wt%, there is an increase in the halo region and a reduction in the crystalline peaks' intensity.

Morphological studies

Figure 5 shows that SEM images of pure P(VDF-TrFE), PFE5fM, and polymer composite films with different wt% of MIL. Figure 5a shows the pristine polymer film with voids. The addition of f-MWCNTs to the polymer, Fig. 5b, shows uniform dispersion of the nanotubes (due to ultrasonication before dispersion) as well as enhancement in the voids' size in the composite films. The f-MWCNTs are seen to be completely wrapped by the polymer. Further, on the introduction of MIL to the polymer composite, Fig. 5c-e, it can be seen that the voids are maximum for 30 wt% of MIL content and minimum for 20 wt%. It is worth mentioning that the cubes observed in the PFE5fM10MIL polymer composite (Fig. 5c) are that of FeCl_3 whose signature is also seen in the XRD pattern (marked by *). The FeCl_3 formation is attributed to the reduction of the MIL's anions.

The porosity of the polymer composites has been measured by BET technique. Worth noting is the fact that although the pore size is minimum for 20 wt% of MIL, Fig. 5d, the pore area is maximum for this composition (as listed in Table 3). These observations of surface morphology and porosity have resulted in enhanced EMI shielding by films with 20 wt% of MIL which is explained below in detail in the Section of electrical and shielding studies. When MIL is added to the polymer composite system, the molecules of MIL can either get attached at the pore openings or at the surface considerably changing (decreasing/increasing) the pore parameters like surface area, volumes, etc. of the porous material [48].

FTIR analysis

The ATR spectra of pure [Bmim][FeCl_4], P(VDF-TrFE), PFE5fM and PFE5fM + x wt% MIL (where, x = 10, 20, and 30) have shown in Fig. 6i-ii. Figure 6i shows the ATR spectra of pure MIL and its characteristic vibrations whose assignments are listed in Table 4 [49, 50]. Figure 6ii shows the ATR spectra of pure P(VDF-TrFE) and its composites. The vibrational bands at 840 cm^{-1} , 880 cm^{-1} , 1076 cm^{-1} , 1165 cm^{-1} , 1283 cm^{-1} and 1402 cm^{-1} correspond to the β -phase of P(VDF-TrFE) [51]. With the addition of f-MWCNTs, few β -phase related bands get shifted and become intense. This may be due to the interaction between f-MWCNTs and P(VDF-TrFE) (as already discussed in XRD and SEM).

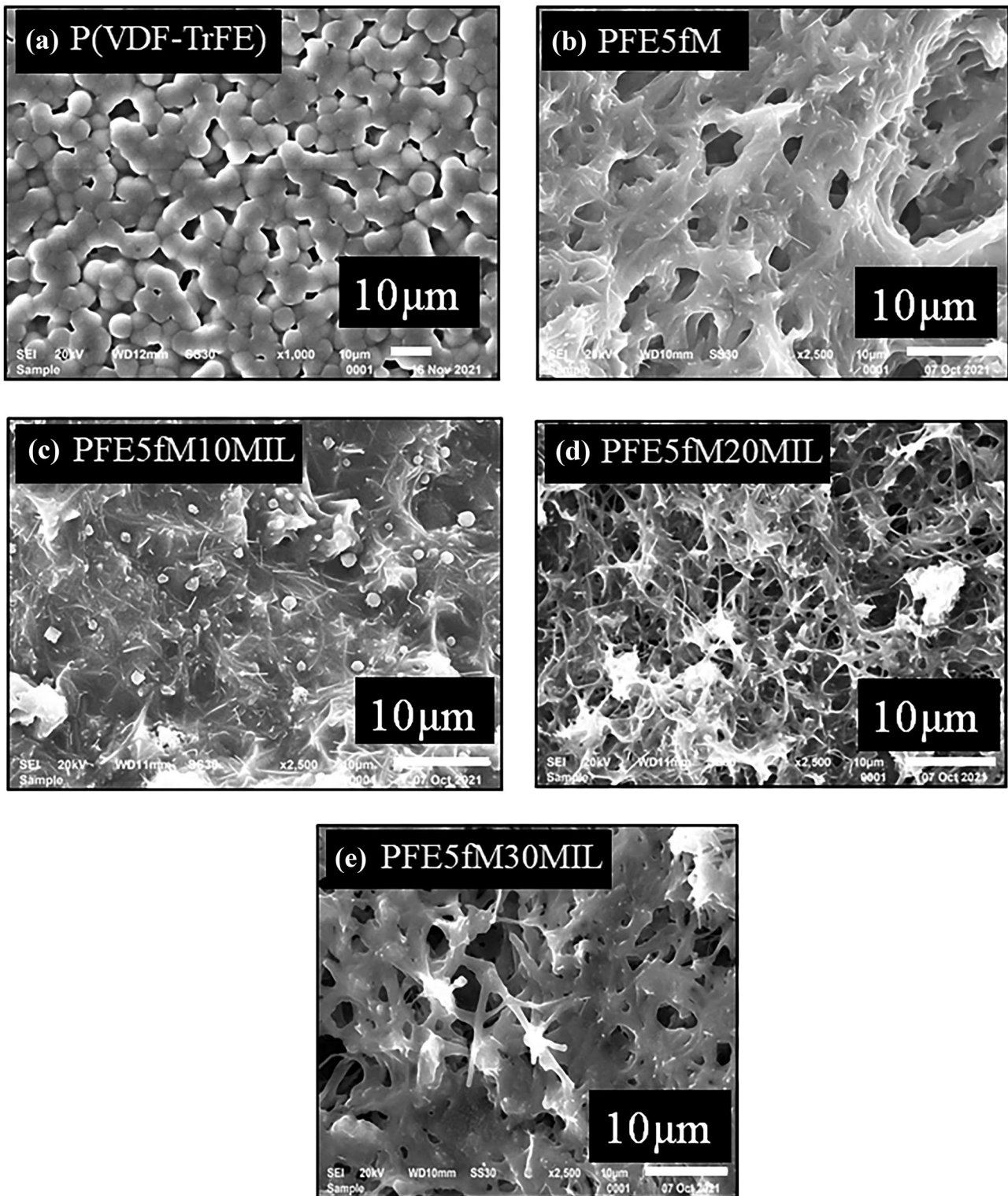


Fig. 5 Surface morphology of polymer composites

The incorporation of MIL (in varying amounts) in the polymer composite is shown in Fig. 6iic, 6iid, & 6iie. The MIL related bands get shifted towards lower wavenumbers

(by $\sim 2\text{--}3\text{ cm}^{-1}$) with increasing content of MIL in the polymer composite. This shift and their corresponding higher intensity is due to the interaction between the MIL and the

Table 3 Raman peaks of polymer composites and intensity ratio I_D/I_G

Samples	Position of D-band (cm^{-1})	Position of G-band (cm^{-1})	Value of R (I_D/I_G)
MWCNTs	1356	1582	0.132
f-MWCNTs	1359	1583	0.133
PFE5fM	1353	1585	0.256
PFE5fM10MIL	1359	1583	0.060
PFE5fM20MIL	1359	1584	0.120
PFE5fM30MIL	1357	1584	0.136

P(VDF-TrFE). Also, the band related to the β -phase of the polymer shifts to lower wavenumbers (listed in Table 4) and becomes prominent with increasing MIL content.

Additionally, some of the characteristic peaks of pure MIL at 619 cm^{-1} , 647 cm^{-1} , 831 cm^{-1} , 1105 cm^{-1} and 1162 cm^{-1} disappear on increasing the MIL content in the polymer composite. This may be due to the complexation between the polymer, f-MWCNTs and MIL [52]. The complexation of f-MWCNTs and the cations/anions of MIL with the polymer backbone is schematically shown in Fig. 7.

Raman studies

Figure 8 shows the Raman peaks of the polymer composites. It is seen that for all the polymer composites containing MIL, the G band shifts towards higher wave number side compared to that of f-MWCNTs while the D band shift

towards the lower wave number side (in Table 2). The shifting of both the D and the G band in the Raman spectra is attributed to the wrapped polymer-MIL complex on the nanotube surface. This has been seen in the SEM images also as discussed earlier. Also, the shift in the G band can be due to a change in the amount and type of chemical groups attached to the functionalized MWCNTs surface which changes the electronic structure of the f-MWCNTs [53]. The complexation between the MIL, f-MWCNTs and polymer matrix can affect the density of electronic states of f-MWCNTs hence requiring higher energy for vibrations resulting in Raman peaks at higher frequency [54, 55].

On addition of 5 wt% of f-MWCNTs in the polymer matrix, the value of R increases as disorder (amorphous region) in the composite increases which is evidenced in SEM also (Fig. 5b) [56]. However, a drop in R value has been seen on the addition of 10 wt% of MIL in PFE5fM polymer composite which is indicative of enhancement in crystallinity in these films attributed to the formation of FeCl_3 crystals explained above in XRD and SEM sections, Figs. 4c and 5c. On further increasing the MIL content ($> 10 \text{ wt}\%$) in the composite, the value of R (Table 2) again increases because of increased amorphicity (reinforced by XRD and SEM, Figs. 4d-e and 5d-e). Also, new peaks are seen at 112 cm^{-1} (Fe-Cl symmetric vibration) and 334.62 cm^{-1} (Fe-Cl symmetric stretch) which are the signatures of FeCl_4^- anions of the MIL [34, 57].

The above obtained results on the polymer composites using XRD, SEM, FTIR, and RAMAN studies are in consonance with each other and further studies given below will throw light on their effective role as EMI shield material.

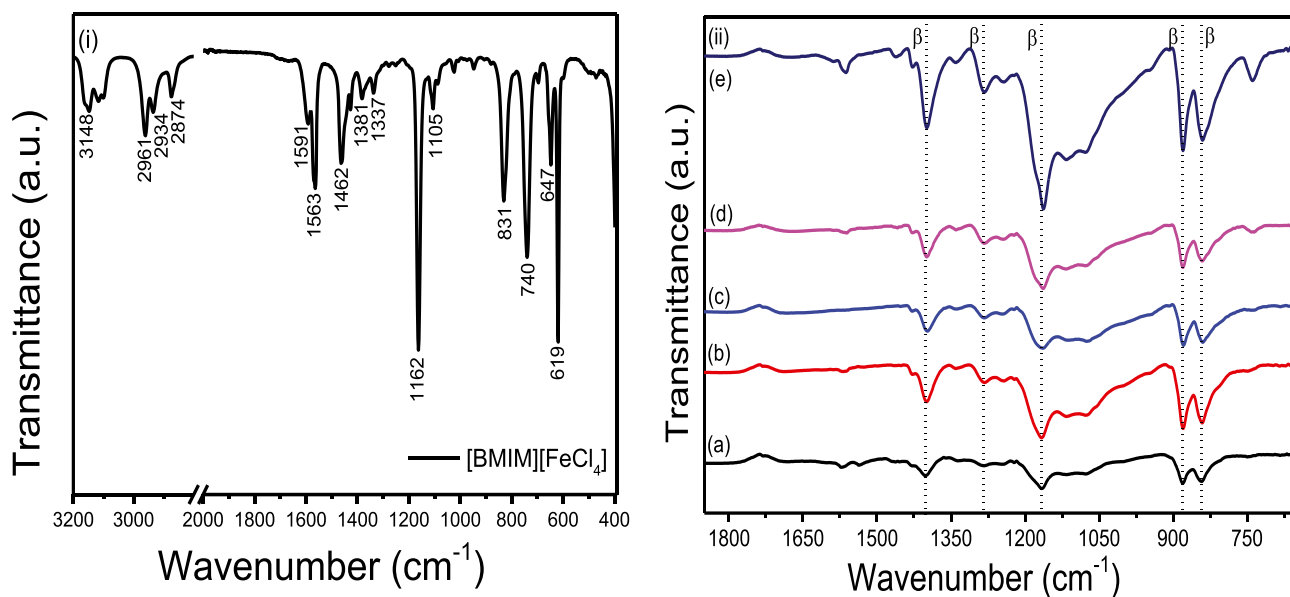


Fig. 6 ATR spectra of **i** pure $[\text{Bmim}][\text{FeCl}_4]$ and **ii** **a** P(VDF-TrFE) **b** PFE5fM, **c** PFE5fM10MIL, **d** PFE5fM20MIL, and **e** PFE5fM30MIL

Table 4 Porosity measurements

Sample	Pore diameter (nm)	Pore area (m ² /g)
PFE5fM	4.04	0.42
PFE5fM10MIL	7.38	1.85
PFE5fM20MIL	5.13	2.50
PFE5fM30MIL	16.93	0.26

Conductivity

Figure 9 shows the room temperature (300 K) conductivity of the polymer composites with MIL incorporated in different wt% (i.e., x wt%, where x = 10, 20, and 30). The conductivity varies with MIL content, being maximum for 20 wt% of MIL. It should be noted that the polymer composite films on addition of MIL become *mixed*, i.e., *electron* (due to MWCNTs) plus *ion* (due to MIL) conductors [58]. Liu et al. [59] and De Volder MFL et al. [60] have reported the electrical conductivity of pristine MWCNT to be $\sim 8 \times 10^8$ S/cm. The polymer composite film with 5 wt% of f-MWCNTs without MIL shows conductivity of ~ 0.65 mS/cm due to the formation of conducting network by f-MWCNTs in polymer matrix. After the addition of 10 wt% of MIL in the composite (PFE5fM), conductivity slightly decreases (~ 0.52 mS/cm) at ambient temperature due to plasticization effect of MIL (which is also reflected in XRD and SEM) which restricts the polymer chain motion

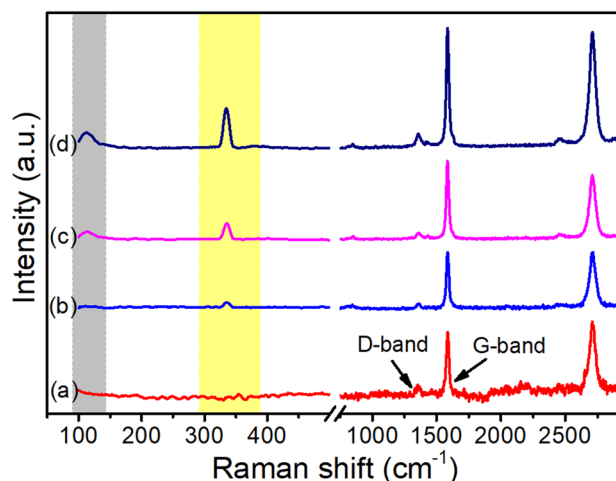


Fig. 8 Raman spectra of **a** PFE5fM, **b** PFE5fM10MIL, **c** PFE5fM20MIL, and **d** PFE5fM30MIL

thereby restricting charge carrier movement. On the incorporation of 20 wt% of MIL to the PFE5fM, the conductivity is found to be maximum (~ 1.77 mS/cm) as a large number of ions of the MIL become available for conduction. However, on the addition of 30 wt% of MIL to the polymer composite, the conductivity slightly reduces (~ 1.24 mS/cm) as the connecting pathway for the charge carriers gets disrupted due to the enhanced pore size of this composite (Fig. 5e) [61].

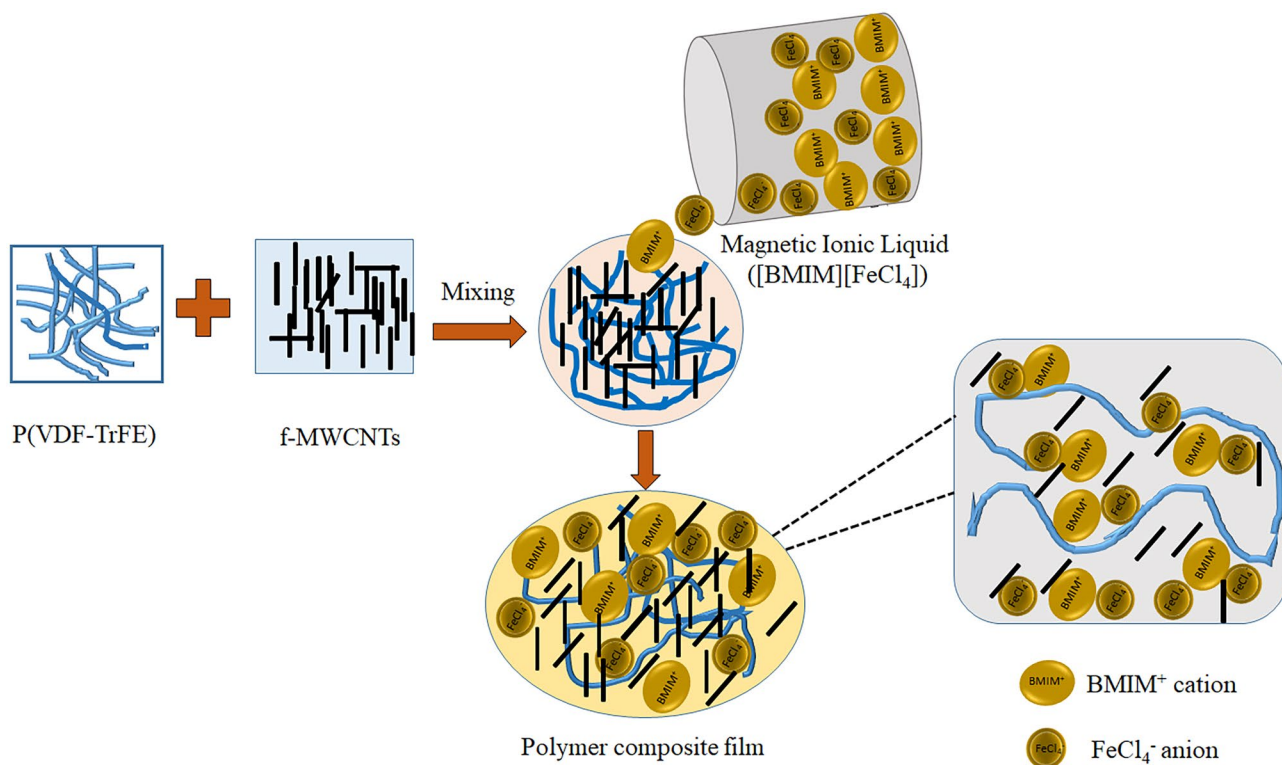


Fig. 7 Schematic representation of interaction of f-MWCNTs and the cations/anions of MIL with the polymer backbone

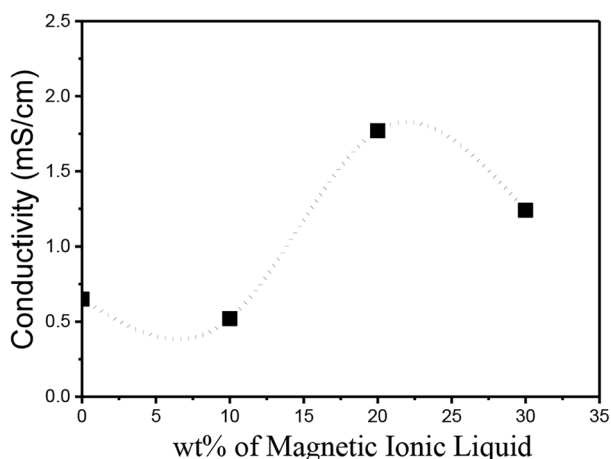


Fig. 9 Conductivity of polymer composites with varying amount of MIL (at room temperature)

TGA studies

Figure 10 shows the TGA curves of the P(VDF-TrFE), PFE5fM, and PFE5fM + x wt% MIL (where, x = 10, 20, and 30). The thermal stability of pristine P(VDF-TrFE) is upto ~410 °C. On the incorporation of f-MWCNTs, the thermal stability further increases to ~430 °C. However, with the introduction of MIL in the PFE5fM composite, the thermal stability decreases to ~350 °C due to the change in the microstructure of the films as MIL addition increases the porosity of the films, destroying the crystalline nature leading to an earlier onset of melting.

All the prepared samples are thermally stable up to ~350 °C which is sufficient for practical applications.

Worth mentioning is the fact that the weight loss at each step in the multi-component system has not been assigned to individual components as the constituents of the polymer

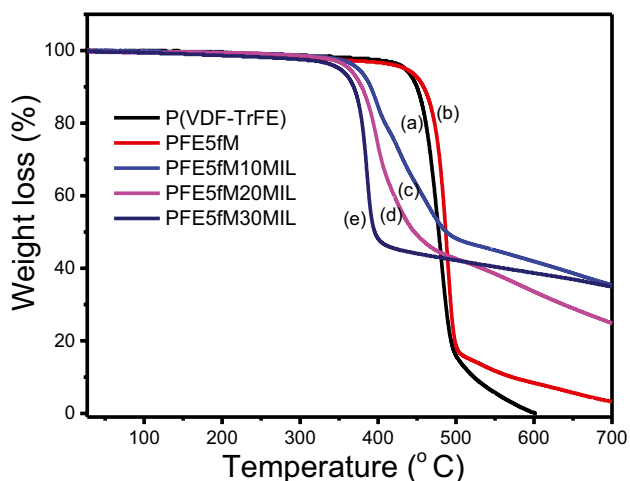


Fig. 10 TGA plots of **a** P(VdF-TrFE), **b** PFE5fM, **c** PFE5fM10MIL, **d** PFE5fM20MIL, and **e** PFE5fM30MIL

composites have varying interactions with each other thereby making it speculative to interpret precisely.

VSM study

Figure 11 shows the magnetic properties of pure MIL, [Bmim][FeCl₄] (inset of Fig. 11) and its composites having different wt% of MIL (10, 20, and 30) (at room temperature). As seen in the inset, the MIL exhibits a linear variation of magnetization with the magnetic field confirming its paramagnetic nature [62]. Similar linear behaviour has been observed for the composite films (with varying MIL content 10–30 wt %). As the MIL content is increased, the saturation magnetization also monotonically increases slightly. Although, the obtained values of saturation magnetization (M_S) are low, they are sufficient to contribute to the EMI shielding effectiveness in terms of magnetic losses.

Electrical and shielding studies

Complex permittivity (ϵ^*) and permeability (μ^*) of polymer composite films are written as

$$\epsilon^* = \epsilon' - i\epsilon'' \quad (1)$$

$$\text{and } \mu^* = \mu' - i\mu'' \quad (2)$$

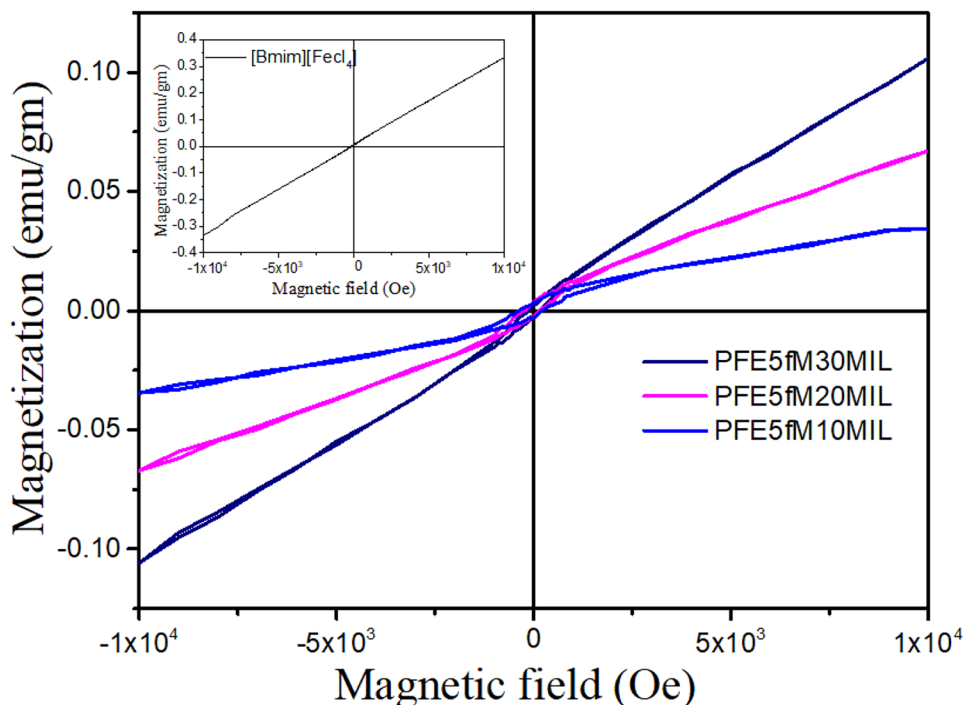
where, ϵ' , μ' and ϵ'' , μ'' , respectively, are storage and loss capability of electric and magnetic energy.

Figure 12i-ii show the frequency dependence of the dielectric constant and dielectric loss of the composite films in the X-band (at 300 K). The dielectric constant is found to be high with 5 wt% f-MWCNTs as compared to the pristine P(VdF-TrFE) as shown in Fig. 12i. This high value of the dielectric constant may be due to the formation of many micro-capacitors between the MWCNTs and the polymer [58]. On incorporation of MIL (10, 20 and 30 wt%) in the polymer composite (PFE5fM), the dielectric constant further increases and is found to be maximum (~228) for PFE5fM-20MIL composite. This enhancement in dielectric constant is attributed to large number of MIL's immobile anions/cations (stored charges) attached to the polymer backbone which do not contribute to the electrical conduction [63]. Consequently, the dielectric loss as well as electrical conductivity reduce as shown in Fig. 12ii & Fig. 14i.

In the polymer composites with and without MIL, dielectric losses (in high and low frequency region) are attributed to the dipolar relaxation and interfacial polarization. Also, the linear behaviour of the dielectric loss at low frequencies in the above polymer composites may be due to conduction of free electrons present at the f-MWCNTs' surface [64, 65].

Figure 13i-ii show the frequency dependence of the real (μ') and imaginary (μ'') parts of the complex permeability.

Fig. 11 Magnetization curves of composite films



The μ' and μ'' of PFE5fM composite without MIL is less than 1 which indicates that this composite has minimal magnetic loss. On incorporation of MIL in PFE5fM, the values of μ' further decreases while μ'' increases as shown in Fig. 13i-ii, respectively. The minimum value of permeability has been obtained for mid-composition, i.e., 20 wt% loading of MIL in the polymer composite (viz., PFE5fM-20MIL). Although sufficient number of magnetic dipoles are available in this system, the microstructural changes observed (as already discussed in SEM and XRD) obstruct their alignment thereby reducing the permeability.

The effect of incorporating MIL in the PFE5fM is rise in μ' above unity (at low frequencies) along with a slight

increase in μ'' is slightly increased above zero in the entire frequency range. This magnetic loss (μ'') may be a combined effect of the motion of magnetic domains, eddy current losses and natural resonance of ferromagnetic materials [66].

As the microwave absorption by a shield material is due to the dielectric and magnetic losses being complimentary [67–69], the high dielectric constant and high magnetic losses of PFE5fM20MIL should lead to high microwave absorption in this composite film.

Figure 14i shows the frequency dependent electrical conductivity of the composite films at 300 K. Being an insulator, the electrical conductivity of pristine P(VDF-TrFE) obtained is $\sim 10^{-9}$ - 10^{-10} S.cm⁻¹. On dispersion of 5 wt% of

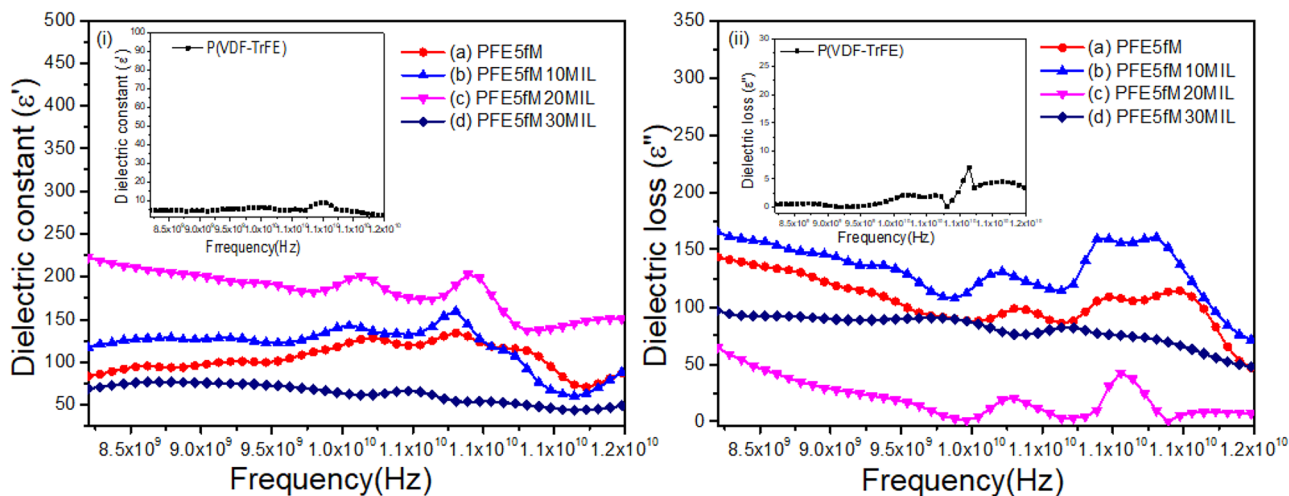


Fig. 12 i Dielectric constant and ii Dielectric loss of P(VDF-TrFE) and its composites

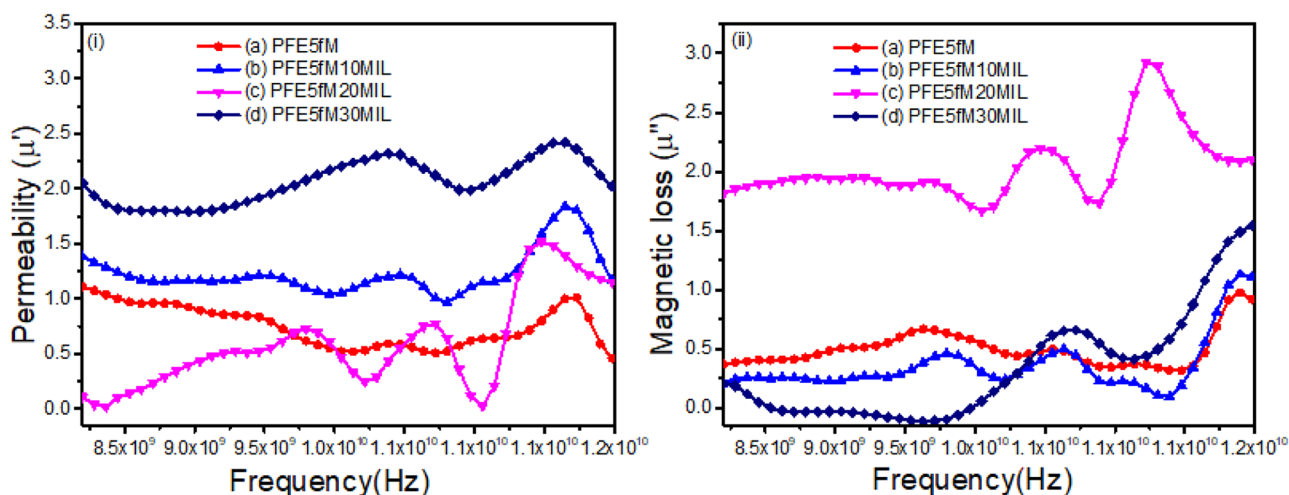


Fig. 13 i Permeability and ii Magnetic loss of P(VDF-TrFE) and its composites

f-MWCNTs, the electrical conductivity increases due to the electrons present in the nanotubes. On the incorporation of 10 wt% of MIL in the PFE5fM system, the electrical conductivity further increases. This is due to the anions/cations of the MIL which make the polymer composites mixed (ion + electron) conductors. However, on addition of 20 wt% of MIL, the conductivity is found to reduce. Microstructure and porosity studies described above indicate at a porous structure with large area for this composition to which this decrement in conductivity is assigned to. The electrical conductivity (σ_{ac}) has been calculated using the following relation;

$$\sigma_{ac} = \omega \epsilon_0 \epsilon'' \quad (3)$$

As seen in this equation, the electrical conductivity depends on the frequency as well as dielectric properties of the material which are being tailored in this study.

A broad peak/hump observed at around 1.05 to 1.18 GHz in all the polymer composites (as shown in Figs. 12 and

13), indicates a resonance behaviour which is expected when the composite films are highly conducting and skin effect becomes significant [34].

Another parameter which needs to be taken into consideration while designing a microwave shield is the skin depth. The skin depth (δ) has been determined using the following equation,

$$\delta = \left(\frac{2}{\mu' \omega \sigma_{ac}} \right)^{0.5} \quad (4)$$

Where, ω , σ_{ac} , and μ' , respectively, are the angular frequency, total electrical conductivity, and relative permeability of the sample. For PFE5fM, a sample with no MIL but electronic conduction, the skin depth is very small. On addition 10 and 30 wt% of MIL to the polymer composite, the value of skin depth does not change much as the conductivity is due to both electrons and ions in these systems. The skin depth is found to be maximum ($\sim 18.38 \mu\text{m}$) for PFE5fM20MIL polymer composite at 8.2 GHz frequency (as both the conductivity

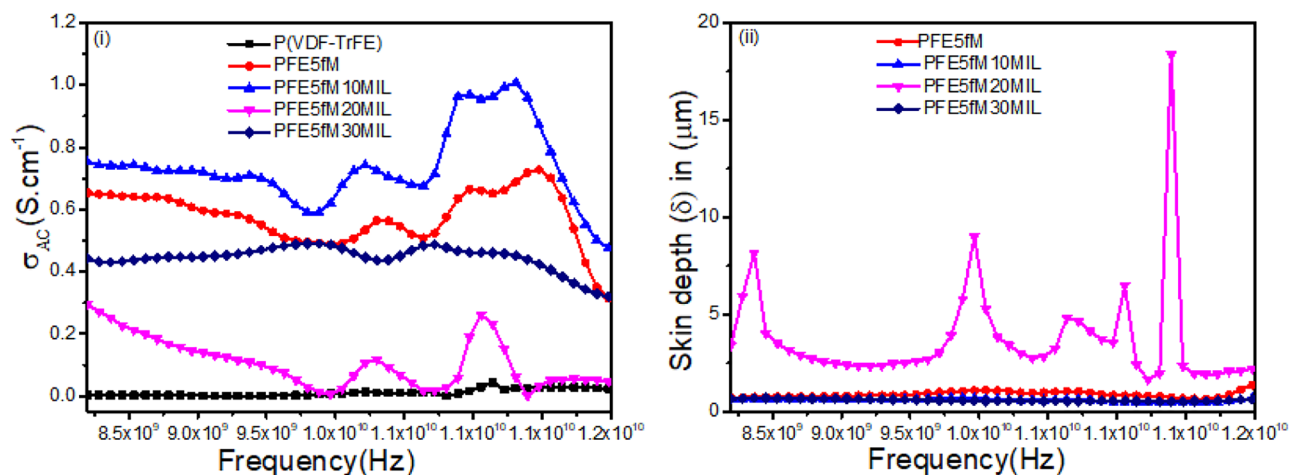


Fig. 14 i Frequency dependent conductivity ii Skin depth of P(VDF-TrFE) and its composites

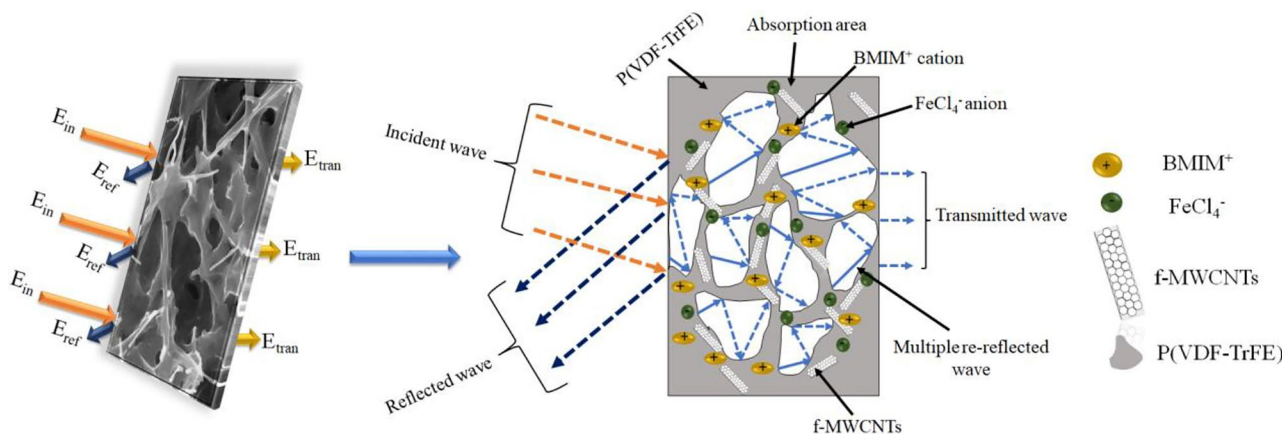


Fig. 15 Schematic representation of EMI shielding mechanism in porous polymer composite film

as well as permeability (μ') decrease here). The variation in skin depth with frequency is shown in Fig. 14ii.

EMI shielding performance and mechanism

Shielding effectiveness (SE) is the ability of shielding material to shield against external EM wave and is evaluated using the equation given below;

$$SE_{P_T}^* = 10 \log\left(\frac{P_{in}}{P_{out}}\right) \tag{5}$$

In this equation, P_{in} and P_{out} are the power (electrical field strength) of the incident and transmitted EM waves, respectively. The overall shielding effectiveness (SE_T) in terms of reflection loss (SE_R), absorption loss (SE_A), and multiple reflection loss (SE_M) is given by the equation;

$$SE_T = (SE_R + SE_A + SE_{MR})(dB) \tag{6}$$

Multiple reflection becomes insignificant and is generally neglected when the absorption loss (SE_A) is greater than 10

dB. Multiple reflection also depends on the skin depth (and hence thickness) of the shield materials. It is well known that multiple reflected waves can be absorbed by the shield material whose thickness is greater than skin depth ($t > \delta$) [70].

Electromagnetic parameters (S-parameters) are associated with the reflectance ($R = |S_{11}|^2 = |S_{22}|^2$), transmittance ($T = |S_{12}|^2 = |S_{21}|^2$) and absorbance ($A = 1 - R - T$). These electromagnetic parameters have been obtained experimentally using the Vector Network Analyzer in the X-band.

The total EMI shielding has been calculated adding the contributions of reflection (SE_R) and absorption (SE_A) by using the equations;

$$SE_R = -10 \log(1 - R) \tag{7}$$

$$SE_A = -10 \log\left(\frac{T}{1 - R}\right) \tag{8}$$

Generally, electromagnetic (EM) radiation is reflected from conducting materials and the extent of reflection depends on the electrical conductivity and morphology of shield material whereas the absorption of EM waves can be controlled

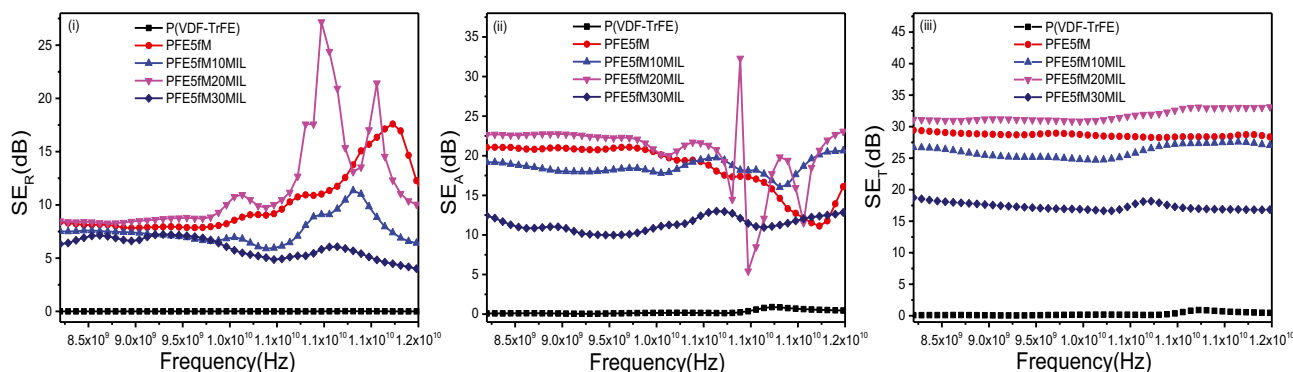


Fig. 16 EMI SE of the polymer composite with different wt % of MIL in X-band (8.2-12.4 GHz)

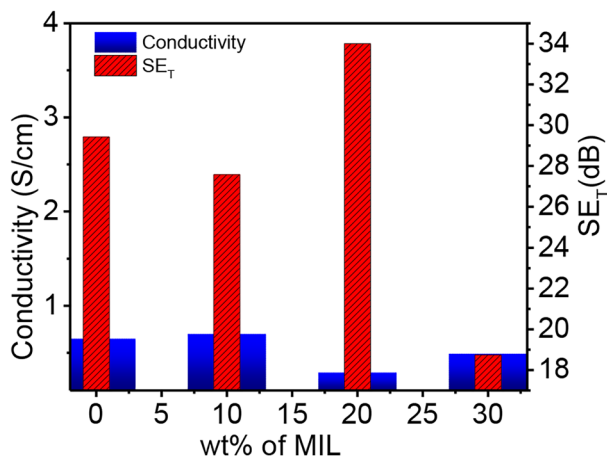


Fig. 17 Conductivity and SE_T of polymer composite films

by the magnetic and dielectric properties of the shield materials. In porous polymer composites, the various interfaces provide different conducting paths to the charge carriers due to the heterogeneity in the materials. These interfaces give rise to multiple-reflections thereby improving the microwave attenuation of EM waves. These porous structures increase the path of EM wave propagation in the material contributing to high EM wave absorption [71]. With changing wt% of MIL, the pores' size and area in the films change too which has been confirmed by BET measurement (as discussed above).

In brief, EMI shielding comprises of *reflection loss* generated on the surface of the shield material, *absorption loss* generated inside the shield material and *multiple reflection loss* generated between interfaces.

The schematic description of electromagnetic wave traveling across a porous polymer composite is shown in Fig. 15.

Figure 16i-iii represent the SE_R, SE_A, and SE_T of the composite films in the X-band (8.2–12.4 GHz). In consonance with the dielectric constant, magnetic loss and conductivity observations given above, maximum shielding effectiveness had been obtained in PFE5fM20MIL (SE_A ~ 24 dB and SE_R ~ 10 dB at a frequency of 1.23 GHz). Worth noting is the fact that the SE_A values are much higher than SE_R values as seen in Fig. 16i-ii which was aimed at in this study, i.e., absorption was the dominant factor in the shielding mechanism. Also, due to the porous structure of the films, multiple reflection also plays an important role in enhancing the SE_T along with the factors mentioned above.

Figure 17 shows the conductivity and total EMI shielding effectiveness of the polymer composites with and without MIL. In PFE5fM20MIL composite film, as the pore area increases, the conductivity decreases due to connecting network being hindered. This enhanced pore area facilitates multiple reflection which ultimately enhances the SE_T. On the addition of 30 wt%

of MIL in the polymer composite, while the pore size increases yet the conductivity also increases due to large number of anions/cations of the MIL. The decrement in the magnetic losses in this film decreases the EMI shielding capability.

Conclusion

In this paper, a shielding material with only three constituents {P(VDF-TrFE), f-MWCNTs and MIL} which is flexible, lightweight and a good microwave absorber in the X-band (8.2–12.4 GHz) has been reported. Here, the magnetic ionic liquid besides being responsible for the enhanced magnetic loss also becomes a source for ionic charge carriers (thereby reducing the need for adding another salt or ionic liquid for conductivity modification). Most studies reported on polymer composites as EMI shields have constituents more than three making their synthesis tedious and expensive. This has been taken care of by the dual role played by the magnetic ionic liquid. Also, the porosity introduced due to the incorporation of MIL in polymer composites results in increased skin depth. All these features add up to give a shield material with maximum SE_T ~ 34 dB (PFE5fM20MIL).

Acknowledgements Financial support from University of Delhi, Institution of Eminence (Ref. No./IoE/2021/12/FRP) and the Alexander von Humboldt Foundation (through its Research Group Linkage programme) is gratefully acknowledged. Also, thanks to CSIR, New Delhi, India for providing the financial support (09/045(1600)/2018-EMR-1) to one of the authors (Anjana). Prof. S. A. Hashmi, Department of Physics & Astrophysics, Mr. Ravinder Singh and Mr. Govind Singh, Department of Chemistry University of Delhi for providing BET, XRD and TGA facilities are gratefully acknowledged. Authors also thank the University Science Instrumentation Centre (USIC), University of Delhi for providing the characterization facilities.

Declarations

Competing interest The authors declare that there are no known competing economic benefits that may affect the studies reported in this paper.

References

- Xu YT, Wang Y, Zhou CG, Sun WJ, Dai K, Tang JH, Lei J, Yan DX, Li ZM (2020) An electrically conductive polymer composite with a co-continuous segregated structure for enhanced mechanical performance. *J Mater Chem A* 8:11546–11554
- Yao Y, Jin S, Zou H, Li L, Ma X, Lv G, Gao F, Lv X, Shu Q (2021) Polymer-based lightweight materials for electromagnetic interference shielding: a review. *J Mater Sci* 56:6549–6580
- Kruželák J, Kvasničáková A, Hložeková K, Hudec I (2021) Progress in polymers and polymer composites used as efficient materials for EMI shielding. *Nano Adv* 3:123–172
- Osawa Z, Kuwabara S (1992) Thermal stability of the shielding effectiveness of composites to electromagnetic interference. Effects of matrix polymers and surface treatment of fillers. *Poly Deg Stab* 35:33–43

5. Kim BR, Lee HK, Kim E, Lee SH (2010) Intrinsic electromagnetic radiation shielding/absorbing characteristics of polyaniline-coated transparent thin films. *Syn Met* 160:1838–1842
6. Hsiao ST, Ma CCM, Tien HW, Liao WH, Wang YS, Li SM, Huang YC (2013) Using a non-covalent modification to prepare a high electromagnetic interference shielding performance graphene nanosheet/water-borne polyurethane composite. *Carbon* 60:57–66
7. Verma M, Chauhan SS, Dhawan SK, Choudhary V (2017) Graphene nanoplatelets/carbon nanotubes/polyurethane composites as efficient shield against electromagnetic polluting radiations. *Comp Part B: Eng* 120:118–127
8. Wu J, Chung DDL (2008) Combined use of magnetic and electrically conductive fillers in a polymer matrix for electromagnetic interference shielding. *J Ele Mater* 37:1088–1094
9. Cao WQ, Wang XX, Yuan J, Wang WZ, Cao MS (2015) Temperature dependent microwave absorption of ultrathin graphene composites. *J Mater Chem C* 3:10017–10022
10. Lü Y, Wang Y, Li H, Lin Y, Jiang Z, Xie Z, Kuang Q, Zheng L (2015) MOF-derived porous Co/C nanocomposites with excellent electromagnetic wave absorption properties. *ACS Appl Mater Interfaces* 7:13604–13611
11. Kim HM, Kim K, Lee CY, Joo J, Cho SJ, Yoon HS, Pejaković DA, Yoo JW, Epstein AJ (2004) Electrical conductivity and electromagnetic interference shielding of multiwalled carbon nanotube composites containing Fe catalyst. *Appl Phys Lett* 84:589–591
12. Che RC, Peng LM, Duan XF, Chen Q, Liang AX (2004) Microwave absorption enhancement and complex permittivity and permeability of Fe encapsulated within carbon nanotubes. *Adv Mater* 16:401–405
13. Kallumottakkal M, Hussein MI, Haik Y, Abdul Latif TB (2021) Functionalized-CNT polymer composite for microwave and electromagnetic shielding. *Polymers* 13:3907
14. Gao R, Ramirez SM, Ingfield DL, Bodnar RJ, Long TE (2013) The preparation of cation-functionalized multi-wall carbon nanotube/sulfonated polyurethane composites. *Carbon* 54:133–142
15. Hsiao ST, Ma CCM, Tien HW, Liao WH, Wang YS, Li SM, Yang CY, Lin SC, Yang RB (2015) Effect of covalent modification of graphene nanosheets on the electrical property and electromagnetic interference shielding performance of a water-borne polyurethane composite. *ACS Appl Mater Interfaces* 7:2817–2826
16. Gui H, Xu P, Hu Y, Wang J, Yang X, Bahader A, Ding Y (2015) Synergistic effect of graphene and an ionic liquid containing phosphonium on the thermal stability and flame retardancy of polylactide. *RSC Adv* 5:27814–27822
17. Hu Y, Xu P, Gui H, Yang S, Ding Y (2015) Effect of graphene modified by a long alkyl chain ionic liquid on crystallization kinetics behavior of poly (vinylidene fluoride). *RSC Adv* 5:92418–92427
18. Xu P, Wang X, Hu Y, Ding Y (2016) Piezoresistive properties of nanocomposites based on silicone rubber and ionic liquid-functionalized carbon black. *Mater Lett* 182:218–222
19. Kumar R, Sahoo S, Joanni E, Singh RK, Tan WK, Kar K, Matsuda A (2021) Recent progress on carbon-based composite materials for microwave electromagnetic interference shielding. *Carbon* 177:304–331
20. Lee S, Jo I, Kang S, Jang B, Moon J, Park JB, Lee S, Rho S, Kim Y, Hong BH (2017) Smart contact lenses with graphene coating for electromagnetic interference shielding and dehydration protection. *ACS Nano* 11:5318–5324
21. Zhang QM, Bharti V, Kavarnos G (2002) Poly (vinylidene fluoride)(PVDF) and its copolymers. *Encyc Smart Mater*
22. Xia W, Zhang Z (2018) PVDF-based dielectric polymers and their applications in electronic materials. *Dielectrics* 1:17–31
23. Nalwa HS (1995) *Ferroelectric polymers: chemistry: physics, and applications*. CRC Press
24. Klein RJ, Runt J, Zhang QM (2003) Influence of crystallization conditions on the microstructure and Electromechanical Properties of Poly (vinylidene fluoride – trifluoroethylene – chlorofluoroethylene) terpolymers. *Macromolecules* 36:7220–7226
25. Lu Y, Claude J, Norena-Franco LE, Wang Q (2008) Structural dependence of phase transition and dielectric relaxation in ferroelectric poly (vinylidene fluoride – chlorotrifluoroethylene – trifluoroethylene) s. *J Phys Chem B* 112:10411–10416
26. Martins P, Lopes AC, Lanceros-Mendez S (2014) Electroactive phases of poly (vinylidene fluoride): determination, processing and applications. *Progress Poly Sci* 39:683–706
27. Wang CC, Song JF, Bao HM, Shen QD, Yang CZ (2008) Enhancement of electrical properties of ferroelectric polymers by polyaniline nanofibers with controllable conductivities. *Adv Funct Mater* 18:1299–1306
28. Santos E, Albo J, Irabien A (2014) Magnetic ionic liquids: synthesis, properties and applications. *RSC Adv* 4:40008–40018
29. Calabria L, Fernandes JA, Migowski P, Bernardi F, Baptista DL, Leal R, Grehl T, Dupont J (2017) Confined naked gold nanoparticles in ionic liquid films. *Nanoscale* 9:18753–18758
30. Joseph A, Żyła G, Thomas VI, Nair PR, Padmanabhan AS, Mathew S (2016) Paramagnetic ionic liquids for advanced applications: a review. *J Mole Liquids* 218:319–331
31. Santos E, Albo J, Irabien A (2014) Magnetic ionic liquids: synthesis, properties and applications. *RSC Adv* 4:40008–40018
32. Cruz MM, Borges RP, Godinho M, Marques CS, Langa E, Ribeiro APC, Lourenço MJV, Santos FJV, de Castro CN, Macatrão M, Tariq M, Rebelo LPN (2013) Thermophysical and magnetic studies of two paramagnetic liquid salts: [C₄mim][FeCl₄] and [P₆₆₆₁₄][FeCl₄]. *Flui Phase Equi* 350:43–50
33. Ribeiro C, Costa CM, Correia DM, Nunes-Pereira J, Oliveira J, Martins P, Gonçalves R, Cardoso VF, Lanceros-Mendez S (2018) Electroactive poly (vinylidene fluoride)-based structures for advanced applications. *Nat Protoc* 13:681–704
34. Kowsari E, Mohammadi M (2016) Synthesis of reduced and functional graphene oxide with magnetic ionic liquid and its application as an electromagnetic-absorbing coating. *Comp Sci Tech* 126:106–114
35. Sanoja-López KA, Quiroz-Suárez KA, Dueñas-Rivadeneira AA, Maddela NR, Montenegro MC, Luque R, Rodríguez-Díaz JM (2022) Polymeric membranes functionalized with nanomaterials (MP@NMs): A review of advances in pesticide removal. *Environ Res* 114776
36. Wang C, Murugadoss V, Kong J, He Z, Mai X, Shao Q, Chen Y, Guo L, Liu C, Angaiah S, Guo Z (2018) Overview of carbon nanostructures and nanocomposites for electromagnetic wave shielding. *Carbon* 140:696–733
37. Sankaran S, Deshmukh K, Ahamed MB, Pasha SK (2018) Recent advances in electromagnetic interference shielding properties of metal and carbon filler reinforced flexible polymer composites: a review. *Comp Part A: Appl Sci Manu* 114:49–71
38. Farbod M, Tadavani SK, Kiasat A (2011) Surface oxidation and effect of electric field on dispersion and colloids stability of multiwalled carbon nanotubes. *Coll Surf A: Physico Eng Asp* 384:685–690
39. Dandekar A, Baker RTK, Vannice MA (1998) Characterization of activated carbon, graphitized carbon fibers and synthetic diamond powder using TPD and DRIFTS. *Carbon* 36:1821–1831
40. do Amaral Montanheiro TL, Cristóvão FH, Machado JPB, Tada DB, Durán N, Lemes AP (2015) Effect of MWCNT functionalization on thermal and electrical properties of PHBV/MWCNT nanocomposites. *J Mater Research* 30:55–65
41. Rath SK, Dubey S, Kumar GS, Kumar S, Patra AK, Bahadur J, Singh AK, Harikrishnan G, Patro TU (2014) Multi-walled CNT-induced phase behaviour of poly (vinylidene fluoride) and its electro-mechanical properties. *J Mater Sci* 49:103–113
42. Jorio A, Dresselhaus G, Dresselhaus MS, Souza M, Dantas MSS, Pimenta MA, Rao AM, Saito R, Liu C, Cheng HM (2000) Polarized Raman study of single-wall semiconducting carbon nanotubes. *Phys Rev Lett* 85:2617
43. Datsyuk V, Kalyva M, Papagelis K, Parthenios J, Tasis D, Siokou A, Kallitsis I, Galiotis C (2008) Chemical oxidation of multi-walled carbon nanotubes. *Carbon* 46:833–840

44. Dresselhaus MS, Dresselhaus G, Jorio A, Souza Filho AG, Saito R (2002) Raman spectroscopy on isolated single wall carbon nanotubes. *Carbon* 40:2043–2061
45. Scheibe B, Borowiak-Palen E, Kalenczuk RJ (2010) Oxidation and reduction of multiwalled carbon nanotubes—preparation and characterization. *Mater Character* 61:185–191
46. Murphy H, Papakonstantinou P, Okpalugo TT (2006) Raman study of multiwalled carbon nanotubes functionalized with oxygen groups. *J Vac Sci Tech B: Micro Nano Stru Proce Measu Pheno* 24:715–720
47. Wang F, Kong Y, Liu Z, Zhu H (2017) All-organic poly (butyl methacrylate)/Poly (vinylidene fluoride-trifluoroethylene) dielectric composites with higher permittivity and low dielectric loss for Energy Storage Application. *Poly Plas Tech Eng* 56:526–534
48. Durak Ö, Zeeshan M, Habib N, Gülbalkan HC, Alshuhle AA, Çağlayan HP, Kurtoğlu-Öztulum SF, Zhao Y, Haşlak ZP, Uzun A, Keskin S (2022) Composites of porous materials with ionic liquids: synthesis, characterization, applications, and beyond. *Microporous Mesoporous Mater* 332:111703
49. Yoshida Y, Otsuka A, Saito G, Natsume S, Nishibori E, Takata M, Sakata M, Takahashi M, Yoko T (2005) Conducting and magnetic properties of 1-ethyl-3-methylimidazolium (EMI) salts containing paramagnetic irons: liquids [EMI][M^{III}Cl₄](M = Fe and FeO. 5GaO. 5) and solid [EMI]₂[Fe^{II}Cl₄]. *Bulle Chem Soci Japan* 78:1921–1928
50. Xie ZL, Jeličić A, Wang FP, Rabu P, Friedrich A, Beuermann S, Taubert A (2010) Transparent, flexible, and paramagnetic ionogels based on PMMA and the iron-based ionic liquid 1-butyl-3-methylimidazolium tetrachloroferrate (III)[Bmim][FeCl₄]. *J Mater Chem* 20:9543–9549
51. Mayeen A, Kala MS, Jayalakshmy MS, Thomas S, Philip J, Rouxel D, Bhowmik RN, Kalarikkal N (2019) Flexible and self-standing nickel ferrite–PVDF–TrFE cast films: promising candidates for high-end magnetoelectric applications. *Dalt Trans* 48:16961–16973
52. Prasanna CM, Suthanthiraraj SA (2016) Effective influences of 1-ethyl-3-methylimidazolium bis (trifluoromethylsulfonyl) imide (EMIMTFSI) ionic liquid on the ion transport properties of microporous zinc-ion conducting poly (vinyl chloride)/poly (ethyl methacrylate) blend-based polymer electrolytes. *J Poly Research* 23:1–17
53. Skakalova V, Kaiser AB, Dettlaff-Weglikowska U, Hrnčarikova K, Roth S (2005) Effect of chemical treatment on electrical conductivity, infrared absorption, and Raman spectra of single-walled carbon nanotubes. *J Phy Chem B* 109:7174–7181
54. Dresselhaus MS, Jorio A, Hofmann M, Dresselhaus G, Saito R (2010) Perspectives on carbon nanotubes and graphene Raman spectroscopy. *Nano Lett* 10:751–758
55. Wang Y, Iqbal Z, Mitra S (2006) Rapidly functionalized, water-dispersed carbon nanotubes at high concentration. *J Ame Chem Soci* 128:95–99
56. Zhang D, Dong QQ, Wang X, Yan W, Deng W, Shi LY (2013) Preparation of a three-dimensional ordered macroporous carbon nanotube/polypyrrole composite for supercapacitors and diffusion modeling. *J Phy Chem C* 117:20446–20455
57. Liu H, Zhao R, Song X, Liu F, Yu S, Liu S, Ge X (2017) Lewis acidic ionic liquid [Bmim] FeCl₄ as a high efficient catalyst for methanolysis of poly (lactic acid). *Catal Lett* 147:2298–2305
58. Vyas MK, Chandra A (2016) Ion–electron-conducting polymer composites: promising electromagnetic interference shielding material. *ACS Appl Mater Interfaces* 8:18450–18461
59. Chang CM, Liu YL (2011) Electrical conductivity enhancement of polymer/multiwalled carbon nanotube (MWCNT) composites by thermally-induced defunctionalization of MWCNTs. *ACS Appl Mater Interfaces* 3:2204–2208
60. De Volder MFL, Tawfick SH, Baughman RH, Hart AJ (2013) Carbon nanotubes: present and future commercial applications. *Science* 339:535–539
61. Fu J, Li Z, Zhou X, Guo X (2022) Ion transport in composite polymer electrolytes. *Mater Adv* 3:3809–3819
62. Döbbelin M, Jovanovski V, Llarena I, Marfil LJC, Cabañero G, Rodriguez J, Mecerreyes D (2011) Synthesis of paramagnetic polymers using ionic liquid chemistry. *Poly Chem* 2:1275–1278
63. Buraidah MH, Teo LP, Majid SR, Arof AK (2009) Ionic conductivity by correlated barrier hopping in NH₄I doped chitosan solid electrolyte. *Phy B: Cond Matt* 404:1373–1379
64. Pötschke P, Dudkin SM, Alig I (2003) Dielectric spectroscopy on melt processed polycarbonate-multiwalled carbon nanotube composites. *Polymer* 44:5023–5030
65. Dakin TW (2006) Conduction and polarization mechanisms and trends in dielectric. *IEEE Ele Insul Mag* 22:11–28
66. Che RC, Peng LM, Duan XF, Chen Q, Liang AX (2004) Microwave absorption enhancement and complex permittivity and permeability of Fe encapsulated within carbon nanotubes. *Adv Mater* 16:401–405
67. Fan Z, Luo G, Zhang Z, Zhou L, Wei F (2006) Electromagnetic and microwave absorbing properties of multi-walled carbon nanotubes/polymer composites. *Mater Sci Eng B* 132:85–89
68. Li G, Hu GG, Zhou HD, Fan XJ, Li XG (2002) Attractive microwave-absorbing properties of La_{1-x}Sr_xMnO₃ manganite powders. *Mater Chem Phy* 75:101–104
69. Wei J, Liu J, Li S (2007) Electromagnetic and microwave absorption properties of Fe₃O₄ magnetic films plated on hollow glass spheres. *J Magne Magne Mater* 312:414–417
70. Tan YJ, Li J, Cai JH, Tang XH, Liu JH, Hu ZQ, Wang M (2019) Comparative study on solid and hollow glass microspheres for enhanced electromagnetic interference shielding in polydimethylsiloxane/multi-walled carbon nanotube composites. *Comp Part B: Eng* 177:107378
71. Singh AK, Shishkin A, Koppel T, Gupta N (2018) A review of porous lightweight composite materials for electromagnetic interference shielding. *Comp Part B: Eng* 149:188–197

Publisher's Note Springer Nature remains neutral with regard to jurisdictional claims in published maps and institutional affiliations.

Springer Nature or its licensor (e.g. a society or other partner) holds exclusive rights to this article under a publishing agreement with the author(s) or other rightsholder(s); author self-archiving of the accepted manuscript version of this article is solely governed by the terms of such publishing agreement and applicable law.